ISSN (Print) 1226-1750
ISSN (Online) 2233-6656
Journal of Magnetics 28(3), 290-298 (2023) https://doi.org/10.4283/JMAG.2023.28.3.290

Study on the Magnetic Rate Sensitivity and Shear Properties of Magnetorheological Shear Thickening Fluid

Guo-Jun Yu[1]*, Shao-Jie Zhu[1], Cheng-Bin Du[2], Ling-Yun Wang[1], and Jun-Chi Huang[1]

[1]*Faculty of Civil Engineering and Mechanics, Jiangsu University, Zhenjiang, Jiangsu Province 212013, China*
[2]*Department of Engineering Mechanics, Hohai University, Nanjing 210098, China*

(Received 28 September 2022, Received in final form 19 July 2023, Accepted 20 July 2023)

This paper studies magnetic field control and velocity-activated magnetorheological shear thickening fluid (MR-STF). High-concentration STF is composed of nano-sized silica particles suspended in a solvent polyethylene glycol (PEG), and then micron-sized carbonyl iron particles of different mass fractions are added to the STF to manufacture different MR-STF. The rheometer is used to study the viscoelasticity of all four samples. The correlation between dynamic behavior and shear rate, angular frequency, and external magnetic field is studied and discussed. In the lower angular frequency range, the loss modulus is slightly larger than the storage modulus, and MR-STF behaves as a viscoelastic state. After the critical angular frequency, the storage modulus decreases sharply, well below the loss modulus. MR-STF appears in a viscous state and a liquid state. With the start of external field excitation, MR-STF is more inclined to MRF. Finally, the apparent viscosity and shear rate of MR-STF are fitted. The results show that with the increase of magnetic induction strength, the plastic viscosity coefficient of MR fluid increases, the flow characteristic index decreases, and the shear thinning effect becomes more significant.

Keywords: magnetorheological shear thickening fluid, performance analysis, shear thickening effect, shear thinning effect

1. Introduction

Magnetorheological fluids (MRFs) are suspensions formed by micron-sized ferromagnetic particles dispersed in a liquid polymer [1]. The MRFs show Newtonian fluid characteristics under the action of no magnetic field, and their performances change rapidly under the action of the magnetic field, showing solid-like characteristics. The MRFs also have good controllability, fast speed response, and reversible characteristics [2, 3]. This property change of the MRFs is called the magnetorheological effect, which has the characteristics of controllable, fast, low energy consumption, and convenient preparation [4, 5], and which is widely used in the fields of vehicle, building structure, precision material polishing and sealing [6-8]. For the MRFs, the Bingham model, Bivisous model, and Herschel Bulkley model are generally used to describe their rheological behavior [9]. The Bivisous model has abrupt changes in the transition phase of the elasticity and shaping of the MRF, which to a certain extent the rheological behavior of the MRF cannot be accurately described, and the three-parameter Herschel-Bulkley model is complicated to calculate. Therefore, the Bingham model with higher accuracy and simple calculation is often used to describe the rheological behavior of the magnetorheological fluid. In the past ten years, domestic research on MRFs has also achieved many results. Yao Jun *et al.* [10] studied the effect of the iron content of carbonyl iron powder on the shear yield strength of magnetorheological fluids and found that The higher the content, the greater the yield stress. Zhu Wanning *et al.* [11] prepared nano-iron particles prepared by the DC arc plasma method as a dispersed phase to prepare an MRF. Nano-iron particle MRFs has a significant magnetorheological effect, and its sedimentation stability is better than that of carbonyl iron powder MRF.s

The Shear Thickening Fluid (STF) material is a new type of functional material, which is a suspension that consists of a mixture of dispersed phase nanoparticles (e.g., SiO_2) and a dispersing medium (e.g., polyethylene glycol). When the shear rate is low, it deforms very easily and can flow slowly like a liquid. When the shear rate is

*Corresponding author: Tel: +86-182-6195-6886
e-mail: gjyu9@ujs.edu.cn

high, its apparent viscosity increases significantly, becomes viscous, and can even change from a liquid to a solid. In recent years, as people's safety requirements continue to improve, the STF material with its excellent energy attenuation ability has attracted great attention as a convenient and practical protective material, and is gradually being used in the field of human body protection [12-15], Energy-absorbing vibration reduction [16, 17] and other fields. As a new type of intelligent fluid, the STF material can respond to external stimuli such as vibration and shock without the need for an external electromagnetic field [18]. The study of mechanical properties and mechanisms of STF materials has received much attention from researchers [19, 20]. Due to the rapid, significant and reversible changes in their mechanical behaviour under external forces, STFs have great application prospects in the fields of vibration damping and absorption, individual protection and impact resistance [21]. Current research on STFs mainly focuses on their application under shear conditions, while STFs also undergo shear thickening accompanied by fluid-solid transformation under impact conditions [22, 23]. Jiang *et al.* [24] tested the energy attenuation of the stress wave in STFs by using an improved SHPB, which further indicates that STFs have significant energy dissipation capability during impact. Therefore, the application of STFs in the field of impact cushioning is of great practical significance and application value to improve impact resistance.

Therefore, in this paper, we combine the advantages of the MRF material and the STF material to prepare a new smart material with magnetic resonance effect, which can work as a common "speed control" and "fail-safe" material without magnetic field. Compared with the conventional MRF material, the MR-STF has better stability. The MR-STF material hybrid abrasive can be applied for magnetic field assisted polishing [25, 26].

The MR-STF material has better stability than traditional MRF material. This article demonstrates the advantages of the MRF material and the STF material in a combined manner by inserting iron powder into the basic medium of the STF material, which has a reasonable passive response and MR effect in the presence of external magnetic fields. Therefore, The MR-STF material designed in this paper overcomes the above defects and achieves the effects of impact energy dissipation and damping energy dissipation. The document is presented in the following order. Section 2 describes the preparation and performance testing of MR-STF. Section 3 discusses the parameter fitting of the apparent viscosity and shear rate and the rheological properties of the MR-STF material. Section 4 contains the conclusions.

2. Preparation of MR-STF

2.1. Preparation of the main materials

2.1.1. Nano-silica particles, polyethylene glycol

Nanosilica is an amorphous white powder that is non-toxic, odourless and non-polluting. It generally has hydroxyl groups and adsorbed water on the surface. It has the characteristics of small particle size, high purity, low density, large specific surface area and good dispersion. With stability, reinforcement, thixotropy and excellent optical and mechanical properties, it is widely used in ceramics, rubber, plastics, coatings, pigments and catalyst carriers, which is of great significance for upgrading some traditional products [27]. The STF material is mainly affected by its dispersion medium and dispersed phase and exhibits different rheological behaviors, among which the content of dispersed phase particles, particle size and surface properties, and the properties of the dispersion medium will affect the shear thickening behavior of the STF material [28]. Nanosilica as a dispersed phase has a great influence on the properties of the shear thickener. Therefore, the critical viscosity of STF increases with the content of nano-SiO_2 particles; the critical shear rate decreases with the content of nano-SiO_2 particles.

Polyethylene glycol [PEG-200] is a non-toxic and stable organic solvent. It has a wide temperature range, moderate viscosity, can be miscible with many solvents, and has a certain suspension capacity. Polyethylene glycol is the main dispersion medium used in rheological systems currently studied. As an important part of shear thickening fluids, polyethylene glycol has an important influence on the rheological properties of rheological systems [29].

2.1.2. Carbonyl iron particles

Carbonyl iron particles are materials that can quickly respond to changes in the external magnetic field, and can obtain high magnetic induction strength with low loss, that is, the external magnetic field is removed, and the smaller the residual magnetic field, the better the reversible control of the magnetic field. The higher the saturation magnetization of the carbonyl iron particles used, the higher the initial magnetic permeability and the maximum magnetic permeability, and the more obvious the magnetostrictive effect of the prepared magnetorheological material. Common soft magnetic particles are mainly Fe_3O_4, Fe_3N and iron, cobalt, nickel and other particles. Among them, the saturation magnetization of iron-cobalt alloys is the highest, reaching 2.4T, but the price is very expensive [30]. For the same type of soft magnetic particles, the geometric parameters such as size

and shape directly determine the saturation magnetization of the particles, which in turn affects the magnetostrictive effect of magnetorheological materials [29, 30]. At present, most of the soft magnetic particles widely used in the preparation of magnetorheological materials at home and abroad are micron scale carbonyl iron powder, and it has been found that carbonyl iron powder has higher saturation magnetization, which is about 8 % higher than spherical carbonyl iron powder [33].

2.2. Preparation and performance testing

2.2.1. Material composition of MR-STF

STF is composed of nano-sized silica particles and polyethylene glycol suspended in a solvent. The prepared STF and carbonyl iron particles constitute the shear thickening and magnetorheological effects of MR-STF. Different weight fractions of carbonyl iron particles and STF were used to prepare different magnetorheologically thickened fluids. The STF used was based on fumed silica (S5505 from SigmaAldrich), with a primary particle size of 14 nm and a specific surface area of about 200 m^2 /g. The carrier liquid was polyethylene glycol [PEG-200] and the density was 1.113 g/ml (102466, ReagentPlus, purchased from Sigma-Aldrich). Preparation materials and instruments are shown in Fig. 1.

The roles of polyethylene glycol and anhydrous ethanol in STF preparation can be complementary, with the exact impact depending on the specific formulation and application. Polyethylene glycol can provide viscosity and tackiness, improving the spread ability of STF and drug release properties. Anhydrous ethanol can act as a solvent, helping to dissolve the drug and other ingredients into the STF and maintaining the sterility of the preparation process through bactericidal action.

2.2.2. Preparation of MR-STF

(1) Preparation of STF

The preparation of STF is mainly to uniformly disperse the dispersed phase micro-particles into the dispersion medium. In this paper, it is prepared by adding a certain amount of diluent and long-term ultrasonic dispersion. It is mainly divided into the following three steps:

According to the preparation of STF Concentration, calculate the mass of the required dispersion medium and SiO_2 particles separately;

Firstly, a small amount of SiO_2 particles are added into the mixed solution of dispersion medium and a certain amount of anhydrous ethanol diluent for calculation, and then ultrasonic dispersion is carried out until SiO_2 particles are uniformly dispersed, and then repeated addition and ultrasonic dispersion are carried out until the addition of SiO_2 required for calculation is completed;

a. silica b. polyethylene glycol c. carbonyl iron powder d. anhydrous ethanol

e. Vacuum drying oven f. Electric Blender

Fig. 1. (Color online) Experimental materials and instruments.

Vacuum drying at room temperature and then vacuum drying at high temperature (100 ℃), until the added absolute ethanol and a small amount of air bubbles and moisture may be mixed.

(2) Preparation of MR-STF

The carrier liquid was added to the powder, and the two components were mechanically mixed using an agitator for 1 hour. The resulting suspension was then placed in a vacuum chamber for several hours to eliminate air bubbles. Another particle was also used for comparison with the carrier liquid. The silica has a primary particle size of 1 to 5 μm and a density of 2.6 g/ml (S5631, from SigmaAldrich). 20 %, 30 % and 40 % solids were selected for the study. An STF was first prepared, which consisted of nano-silica particles and polyethylene glycol suspended in a solvent. A series of magnetorheological shear thickening fluids were prepared by using carbonyl iron particles and STF with different weight fraction ratios. Carbonyl iron particles with an average particle size of 3.5 μm (carbonyl iron, C3518, Jiangsu Tianyi Ultrafine Metal Powder Co., Ltd.) were selected as the magnetic powder in the magnetorheological fluid. Pre-weighed solid iron microspheres were weighed in an amount added to form several MR-STF weight fraction mixtures. Under mechanical stirring conditions, the granules are thoroughly mixed with the base liquid for about 10 minutes. The resulting mixture was then placed in a vacuum oven to remove excess air bubbles. The four iron particles with different weight ratios of MR-STF are 5 %, 10 %, 20 %, and 30 %. The sample preparation is shown in the following Table 1:

Table 1. Mix proportion of MR-STF samples.

Sample	25%STF (g)	Carbonyl iron particles (g)	Mass fraction of carbonyl iron particles
MR-STF5	20.00	1.05	5%
MR-STF10	20.00	2.22	10%
MR-STF20	20.00	5.00	20%
MR-STF30	20.00	8.57	30%

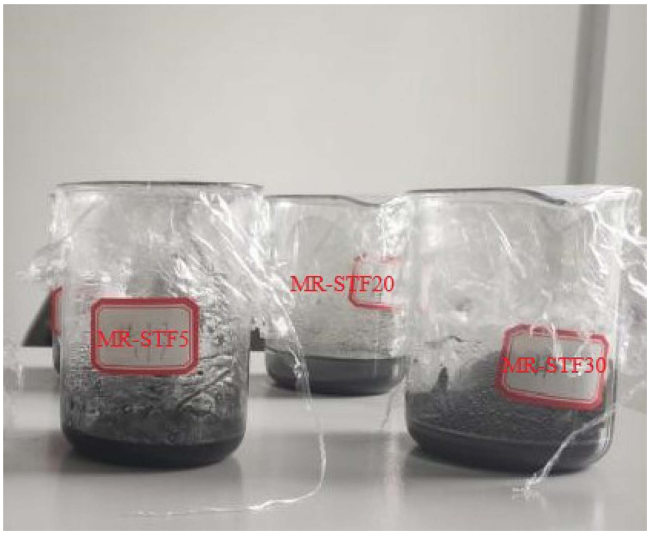

Fig. 2. (Color online) MR-STF samples.

The sample prepared by MR-STF is shown in Fig. 2. Fig. 2 is the schematic diagram of four MR-STF samples of MR-STF5, MR-STF10, MR-STF20 and MR-STF30.

2.2.3. Performance test of MR-STF

The characteristics of MR-STF are characterized by rheological properties, which can be obtained through steady-state rheological performance tests and dynamic rheological tests [29]:

In the steady-state rheological test, a constant shear rate (v) is applied to the sample, and the shear stress in the steady state (τ), the viscosity (η) can be calculated by formula (1):

$$\eta = \frac{\tau}{v} \tag{1}$$

When the viscosity does not change with the shear rate, the fluid is Newtonian fluid; When the viscosity increases, the shear rate increases, and the fluid thickens;If the shear rate decreases, the fluid becomes shear thinner.

In the dynamic rheological test, a sine shear strain (γ) with amplitude (γ_0) and frequency (ω) is applied to the sample, as shown in equation (2):

$$\gamma = \gamma_0 \sin(\omega t) \tag{2}$$

Then the relationship of the shear stress (τ) is in accordance with equation (3), and it is a phase angle (δ) different from the shear strain (γ):

$$\tau = \tau_0 \sin(\omega t + \delta) \tag{3}$$

If the strain amplitude (γ_0) is sufficiently small, then the corresponding linear elastic interval, and the stress (τ) is expressed as equation (4):

$$\tau(t) = \gamma_0 \left[G'(\omega)\sin(\omega t) + G''(\omega)\cos(\omega t) \right] \tag{4}$$

In the formula, $G'(\omega)$ is the storage modulus, which reflects the elasticity of the material; $G''(\omega)$ is the energy dissipation modulus, which reflects the viscosity of the material. When $G'(\omega)$ is much larger than $G''(\omega)$, the material mainly undergoes elastic deformation, which appears to be solid; when $G'(\omega)$ is much smaller than $G''(\omega)$, the material mainly undergoes viscous deformation, which appears to be liquid.

The test conditions are as follows:

(1) Steady-state rheological performance test: When

the test temperature is 25 °C and the shear rate is in the range of 1-1000 s^{-1}, the viscosity of MR-STF samples with different iron particle mass fractions is tested to obtain Relationship between viscosity (Pa·s) and shear rate (1/s).

(2) Dynamic rheological performance test: Under the condition that the test temperature is 25 °C and the strain is 5 %, the angular modulus is in the range of 0.1-100 rad/s, and the storage modulus of MR-STF samples with different mass fractions of iron particles (G') And energy dissipation modulus (G'') to test, get the relationship between modulus (Pa)-angular frequency (rad/s).

2.2.3.1. Analysis of Steady-state Rheological Performance of MR-STF

In this paper, the dynamic performance of MR-STF is tested with the rheometer MCR51. The MCR51 test system is shown in Fig. 3. The dynamic mechanical performance test of MR-STF uses rotary shear mode. The parallel plate rotor (PP20 test head) of the MCR51 rheometer performs rotational shear with a sine wave to test the dynamic mechanical performance of the sample. MCR51 rheometer rotor disk diameter is 20 mm, the magnetic field in the parallel disk gap is generated by the closed magnetic circuit current. To minimize magnetic leakage losses, ensure that the power is less than 15 W. Using this rheometer system, there are two measurement modes, including stress scanning mode and frequency scanning mode, to study the viscoelastic properties of materials. The dynamic performance test of MR-STF is in the steady-state strain rate scanning mode, the shear rate is 1 to 1000 s^{-1}, and 4 different magnetic fields are applied for 0, 0.1, 0.2, and 0.3T. The MCR51 rheometer rotor disc gap is always set at 1.0 mm.

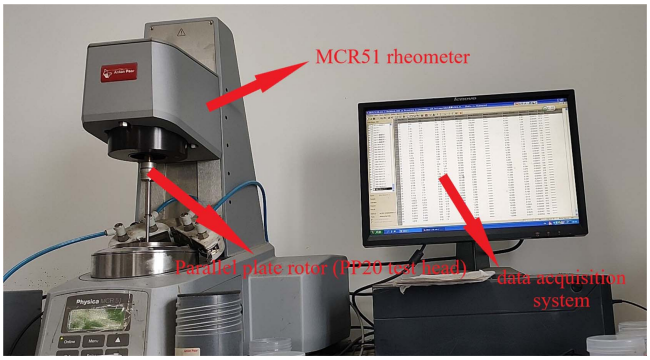

Fig. 3. (Color online) Picture of rheometer testing system.

Figures 4a and 4b show the relationship between the viscosity and the shear rate of the MR-STF sample in the absence and presence of a magnetic field. In Fig. 4a, in the absence of a magnetic field, the low-concentration MR-STF sample shows a shear thickening effect. Except for the sample MR-STF30, its shear thickening effect is not as good as the other three because the iron concentration of MR-STF30 may be high enough to be affected by magnetic fields. Fig. 4b shows the effect of magnetic field strength on the sample in the presence of a magnetic field. The viscosity of the four MR-STF samples increased with increasing magnetic field strength, indicating that all MR-STF samples have obvious MR effects. Only sample MR-STF5 showed weak shear thickening effect, and other samples did not show shear thickening. It can also be seen that the higher the concentration of iron particles, the stronger the MR effect of MR-STF samples and the weaker the shear thickening effect. This can be explained in several ways. First, carbonyl iron particles prevent the movement of fumed

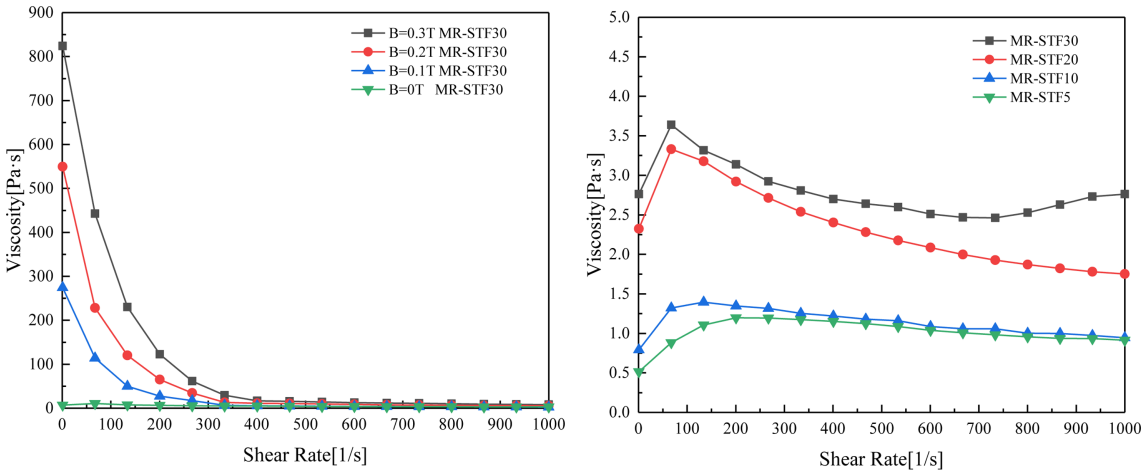

(a) No magnetic field (b) Magnetic field

Fig. 4. (Color online) Viscosity of MR-STF with and without magnetic field changing with shear rate.

silica, so it is difficult for fumed silica to form a thickener to increase the viscosity of the fluid. Then, the higher the MR-STF sample concentration, the lower the fumed silica concentration due to the iron particles in the medium, which also resulted in a weaker shear thickening effect. Carbonyl iron particles also contributed to the increase in the initial viscosity of the MR-STF sample. In the low shear rate range, the higher viscosity value of the MR-STF sample makes its viscosity increase less obvious than before, and it begins to thicken. The critical shear rate of MR-STF may shift to more than 1000 1/s, which cannot be achieved by laboratory rheometers.

MR-STF30 does not show shear thickening effect in Fig. 4(a). It shows shear thickening effect when a magnetic field is applied. The main reasons for this phenomenon may be:

(1) Differences in experimental conditions: the shear thickening effect of MR-STF30 may be very sensitive to experimental conditions. The experimental conditions in Fig. 4(a) may be different from the effect observed when a magnetic field is applied. For example, there may be other factors that affect shear thickening, such as temperature, pressure, or other environmental conditions.

(2) Material differences: MR-STF30 may have a different composition or structure than other MRSTFs, resulting in a different behaviour at zero magnetic field. This may be related to its specific chemical composition, particle shape or dispersion.

In Fig. 4(b), the viscosity of MR-STF30 increases when shear rate rises from 800 to 1000. The main reasons for this phenomenon may be:

(1) Shear rate sensitivity: there may be differences in the response of different magnetorheological fluids to shear rate. Some magnetorheological fluids are more sensitive to shear rate, i.e. they show a greater increase in viscosity at higher shear rates. This may be due to changes in the internal microstructure of the fluid or different responses to interactions between particles.

(2) Changes in flow behaviour: when the shear rate increases, the flow behaviour of the fluid may change. At low shear rates, the microstructure of magnetorheological fluids may be able to adapt to the shear force and show lower viscosity. However, when the shear rate increases, the microstructure of the fluid may not be able to adapt in time, resulting in an increase in viscosity.

Therefore, it can be seen from Fig. 4 that in the absence of a magnetic field, the dynamic properties of MR-STF and STF are very similar. This proves that MR-STF can work as a normal shear thickener without magnetic properties. In the presence of a magnetic field, the results show that the performance of the MR-STF is very different from the case without a magnetic field. The viscosity of MR-STF will increase with the increase of the magnetic field strength, which also proves that MR-STF can work as a normal magnetorheological fluid when it is magnetic. In addition, it can also be seen that under the condition of magnetism, the higher the concentration of iron particles, the stronger the magnetorheological effect of MR-STF, and the shear thickening effect will be relatively weak. These results show that MR-STF has both magneto-rheological effects and shear thickening effects, where the shear thinning effect plays a dominant role in the magnetic field.

2.2.3.2. Dynamic Rheological Performance Analysis of MR-STF

The absolute shear thickening effect (ASTe) and relative shear thickening effect (RSTe) are defined as the performance indexes of MR-STF, as shown in formula (5).

$$ASTe = G'_{\max} - G'_{\min}$$
$$RSTe\% = \frac{G'_{\max} - G'_{\min}}{G'_{\min}} \times 100\% \quad (5)$$

Where G'_{max} is the maximum shear storage modulus of MR-STF under external load, and G'_{min} is the initial shear storage modulus of MR-STF.

Figure 5 shows the change in the storage modulus (G') and loss modulus (G'') of the MR-STF samples with four different iron particle mass fractions at an angular frequency of 0.1-100 rad/s when the strain is 5 %. For the double logarithmic curve, the solid points in the figure represent the storage modulus (G'), and the

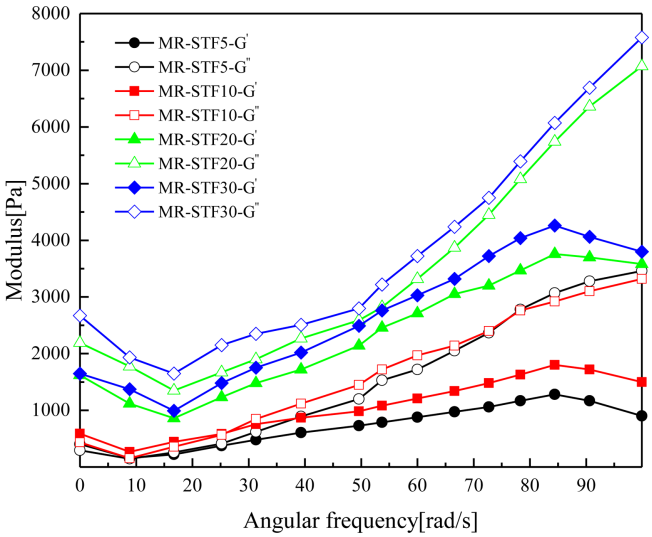

Fig. 5. (Color online) Relationship between modulus and angular frequency of MR-STF at 5 % strain.

hollow points represent the loss modulus (G'').

The absolute shear thickening effect of MR-STF5 is 0.0011 MPa, the relative shear thickening effect is 705 %; the absolute shear thickening effect of MR-STF10 is 0.0015 MPa, the relative shear thickening effect is 579 %; the absolute shear thickening effect of MR-STF20 is 0.0027 MPa, the relative shear thickening effect is 316 %; the absolute shear thickening effect of MR-STF30 is 0.0033 MPa, the relative shear thickening effect is 330 %. It can be seen that the increase of the mass fraction of iron particles is conducive to the enhancement of the absolute shear thickening effect of MR-STF, and the shear storage modulus of MR-STF increases as a whole under the influence of the mass fraction of iron particles. At the same time, It can be seen from the figure that the trends of the modulus curves of MR-STF with different mass fractions are similar. At low angular frequencies, the initial curve has less oscillation due to the instability of the dynamic test. After the dynamic test is stable, as the angular frequency increases, the value of the loss modulus (G'') has been increasing slowly. The storage modulus (G') increases first, and then decreases after reaching the critical angular frequency. In the lower angular frequency range, the loss modulus (G'') is slightly larger than the storage modulus (G'), and the MR-STF behaves as a viscoelastic state; after the critical angular frequency, the storage modulus (G') drops sharply, much lower than loss modulus (G''), MR-STF shows a viscous state and a liquid state, indicating that the MR-STF has shear thinning behavior.

3. Test Results and Discussion

3.1. Apparent viscosity and shear rate parameter fitting of MR-STF

It can be seen from Fig. 4 that the apparent viscosity of MR-STF begins to decrease significantly with increasing shear rate, and then tends to be gentle, and increases with increasing magnetic induction.

The constitutive relationship of MR-STF can be represented by the Bingham model [34], see equation (6).

$$\tau = \tau_0(B)\mathrm{sign}(\nu) + \eta\nu \tag{6}$$

In the formula: τ is the shear stress of MR-STF; B is the magnetic induction strength of the external magnetic field; $\tau_0(B)$ is the yield stress caused by the external magnetic field; η is the viscosity of MR-STF; ν is the shear rate.

Bingham model assumes that the viscosity of MR-STF after yield is constant, but in fact, MR-STF has shear thinning phenomenon. Herschel-Bulkley model explains that the yielding viscosity of MR-STF depends on the shear rate. There is an exponential relationship between them relationship [35], the model can be expressed as:

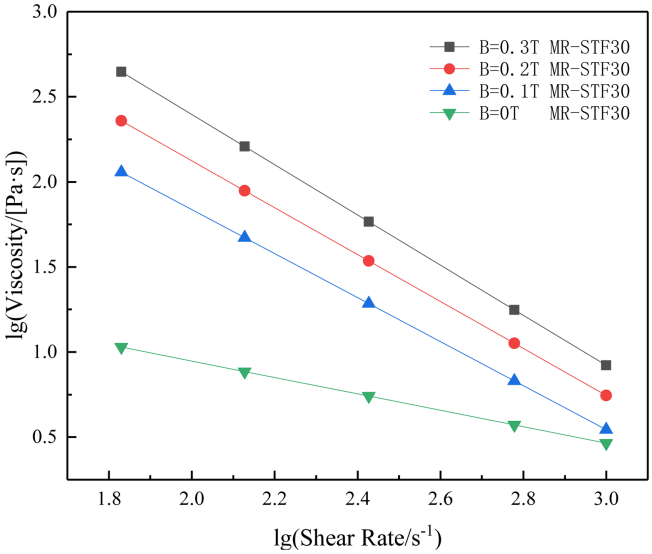

Fig. 6. (Color online) Fitting curve of apparent viscosity and shear rate of MR-STF30 under different magnetic induction intensities.

$$\tau = \left[\tau_0(B) + K\cdot\nu^n\right]\mathrm{sign}(\nu) \tag{7}$$

In the formula: K is the plastic viscosity coefficient of MR-STF; n is the flow characteristic index. The joint equations (6) and (7) show that the relationship between viscosity (η) and shear rate (ν) is:

$$\eta = K\cdot\nu^{n-1} \tag{8}$$

It can be seen from equation (8) that when $n > 1$, the MR-STF has a shear thickening phenomenon; when $n < 1$, the MR-STF has a shear thinning phenomenon; when $n = 1$, the model is equal to the Bingham model.

Equation (8) is used to fit the logarithm of the apparent viscosity and shear rate of the MR-STF30. Figure 6 shows that the apparent viscosity of MR-STF30 and the logarithm of shear rate have a good linear relationship, that is, there is an exponential relationship between the two. As the shear rate increases, the apparent The viscosity decreases exponentially; with the increase of the magnetic induction intensity, the plastic viscosity coefficient of the MR-STF30 increases, the flow characteristic index decreases, and the shear thinning effect becomes more obvious.

It can be seen from Fig. 4 that under different magnetic field strengths, the logarithmic linear relationship between apparent viscosity and shear rate of MR-STF30 is as follows:

① B = 0T, $y = -0.48259x + 1.91244$;

Table 2. Fitting results of apparent viscosity and shear rate.

B/T	R^2	K	n
0	0.48259	1.91244	1.061
0.1	1.29327	4.42425	0.966
0.2	1.37874	4.88169	0.919
0.3	1.47378	5.3429	0.865

② B = 0.1T, $y = -1.29327x + 4.42425$;
③ B = 0.2T, $y = -1.37874x + 4.88169$;
④ B = 0.3T, $y = -1.47378x + 5.3429$.

Therefore, the fitting results of apparent viscosity and shear rate of MR-STF30 are as shown in Table 2.

It can be seen from Table 2 that MR-STF30 has the phenomenon of shear thickening without magnetic field and shear thinning with magnetic field, and the shear thinning effect will become more and more obvious with the increase of magnetic field.

3.2. Rheological properties of MR-STF

As the shear rate increases, the network structure of the MR-STF system itself is gradually destroyed, and some relatively isolated silica aggregates are formed, and the viscosity decreases significantly. When the shear rate reaches the critical shear rate, the fluid force becomes the main force in the MR-STF system, which promotes the secondary agglomeration of relatively isolated silica aggregates in the MR-STF system to form a "particle cluster". The particle cluster becomes larger with the increase of the fluid force, and the hindering effect on the fluid becomes larger. Therefore, at this time, the viscosity of the MR-STF system increases as the shear rate increases.

Shear thickening is a non-Newtonian fluid behavior. The fluid often forms a colloidal suspension. The viscosity of the fluid increases sharply when the shear stress increases rapidly, sometimes discontinuously, and the process is reversible. This phenomenon is mainly attributed to the formation of clusters of particle rigid structures under liquid pressure. A prerequisite for MR-STF thickening is the presence of shear forces.

The MR-STF is a non-Newtonian fluid. As the shear rate changes, the viscosity also changes, and the viscosity itself is also a function. The formula is expressed as follows:

$$\sigma = \eta \cdot \nu \tag{9}$$

σ and ν are macroscopically measurable quantities, the viscosity (η) can be expressed as:

$$\eta = \frac{\sigma}{\nu} \tag{10}$$

The change of shear rate will cause the change of η and σ at the same time. The existence of this kind of nonlinearity can make MR-STF thicken rapidly in the limited range of shear rate and meet the protection requirements of a certain level of impact protection facilities. For a given MR-STF, the critical point is a fixed shear rate value, which can also be regarded as a characteristic parameter of the fluid. Only when the shear rate exceeds the critical point of fluid shear thickening can MR-STF appear shear thickening.

4. Conclusion

(1) Under the action of a magnetic field, the shear stress of the MR-STF increases slowly with increasing shear rate, while the apparent viscosity decreases exponentially; at the same shear rate, as the magnetic induction strength increases, Both MR-STF shear stress and apparent viscosity increase, and the shear thinning effect is more pronounced.

(2) The absolute shear thickening effect of MR-STF5 is 0.0011 MPa, the relative shear thickening effect is 705 %; the absolute shear thickening effect of MR-STF10 is 0.0015 MPa, the relative shear thickening effect is 579 %; the absolute shear thickening effect of MR-STF20 is 0.0027 MPa, the relative shear thickening effect is 316 %; the absolute shear thickening effect of MR-STF30 is 0.0033 MPa, the relative shear thickening effect is 330 %. It can be seen that the increase of the mass fraction of iron particles is conducive to the enhancement of the absolute shear thickening effect of MR-STF, and the shear storage modulus of the MR-STF increases as a whole under the influence of the mass fraction of iron particles.

(3) The MR-STF exhibits non-Newtonian fluid properties at low shear rates. As the shear rate increases, the interaction force between the nanoparticles and the dispersed phase polymer chain increases.

(4) The MR-STF is a kind of intelligent material with controllable performance. The research on high-performance MR-STF has a broad prospect in vibration absorption, individual protection, impact resistance and so on, which has great application value.

Conflict of Interests

The authors declare that there is no conflict of interests regarding the publication of this paper.

Acknowledgements

We wish to acknowledge the financial support by the

Primary Research and Development Plan of Jiangsu Province (Grant No. BE2017167) and the Special Fund for Science and Technology Plan of Jiangsu Province (Grant No. BE2022162).

Data Availability Statement

The datasets generated during and/or analysed during the current study are available from the corresponding author on reasonable request.

References

[1] M. Ashtiani, S. H. Hashemabadi, and A. Ghaffari, J. Magn. Magn. Mater. **374**, 716 (2015).
[2] T. Chen, J. M. Ge, C. Lin, et al., J. Sci. Tech. Eng. **18**, 147 (2018).
[3] M. Ashtiani, S. H. Hashemabadi, and A. Ghaffari, J. Magn. Magn. Mater. **374**, 716 (2015).
[4] J. J. Yang, H. Yan, X. M. Wang, et al., J. Func. Mater. **45**, 4095 (2014).
[5] M. Ashtiani, S. H. Hashemabadi, and A. Ghaffari, J. Magn. Magn. Mater. **374**, 716 (2015).
[6] L. Tang, E. Yue, S. A. Luo, et al., J. Func. Mater. **42**, 1065 (2011).
[7] F. Imaduddin, S. Mazlan, and H. Zamzuri, J. Mater Design **51**, 575 (2013).
[8] F. Chen, Z. Z. Tian, and J. Wang, J. Func. Mater. **45**, 20095 (2014).
[9] C. Y. Guo, Ph.D. Theisi, University of Science and Technology of China, China (2013).
[10] J. Yao, J. Q. Zhang, Z. Z. Peng, et al., J. Mater. Res. **28**, 955 (2014).
[11] W. Zhu, Y. Tong, X. Yu, et al., J. Aerosp. Technol. **3**, 56 (2019).
[12] Y. S. Lee, E. D. Wetzel, and N. J. Wagner, J. Mater Sci. **38**, 2825 (2003).
[13] V. B. C. Tan, T. E. Tay, and W. K. Teo, J. Solids Struct. **42**, 1561 (2005).
[14] C. Y. Tham, V. B. C. Tan, and H. P. Lee, J. Impact Eng. **35**, 304 (2008).
[15] Y. Park, Y. H. Kim, A. H. Baluch, et al., J. Compos. Struct. **125**, 520 (2015).
[16] H. Zhou, L. X. Yan, W. F. Jiang, et al., J. Intel. Mat. Syst. Str. **27**, 208 (2016).
[17] F. Y. Yeh, K. C. Chang, T. W. Chen, et al., J. Chin. Inst. Eng. **37**, 983 (2014).
[18] P. Zhao, M. C. Yu, Q. Chen, et al., J. Vib. Eng. **31**, 966 (2018).
[19] I. R. Peters, S. Majumdar, and H. M. Jaeger, J. Nature **532**, 214 (2016).
[20] E. Brown and H. M. Jaeger, J. Rep. Prog. Phys. **77**, 046602 (2014).
[21] H. Zhou, L. X. Yan, W. Q. Jiang, S. H. Xuan, et al., J. Intell. Mater. Syst. Struct. **27**, 208 (2016).
[22] A. S. Lim, S. L. Lopatnikov, N. J. Wagner, et al., J. Rheologica Acta. **49**, 879 (2010).
[23] A. S. Lim, S. L. Lopatnikov, N. J. Wagner, et al., J. Non-newton Fluid **166**, 680 (2011).
[24] W. F. Jiang, X. L. Gong, S. H. Xuan, et al., J. App. Phys. Lett. **102**, 101901 (2013).
[25] Z. Fan, Y. Tian, Q. Zhou, et al., J. Part B: Eng. Manuf. **234**, 1069 (2020).
[26] C. Qian, Y. Tian, Z. Fan, et al., J. Smart Mater Struct. **31**, 095004 (2022).
[27] M. L. Zhang, L. G. Ding, X. Y. Jing, et al., J. Chem. Eng. **99**, 11 (2003).
[28] J. Bender and N. J. Wagner, J. Rheology **40**, 899 (1996).
[29] X. Liu Xu, Ph.D. Theisi, Nanjing University of Aeronautics and Astronautics, China (2018).
[30] Y. Y. Han, G. T. He, Y. C. Lin, et al., J. Func. Mater. **44**, 3513 (2013).
[31] J. D. Vicente, J. P. Segovia-Gutierrez, E. Andablo-Reyes, et al., J. Chem. Phys. **131**, 194902 (2009).
[32] R. V. Upadhyay, Z. Laherisheth, and K. Shah, J. Smart Mater and Struct. **23**, 015002 (2014).
[33] S. T. Shilan, S. A. Mazlan, Y. Ido, et al., J. Smart Mater Struct. **25**, 095025 (2016).
[34] L. A. Berlic, J. Appl. Phys. Lett. **101**, 021903 (2012).
[35] L. J. Xiao, C. P. Wang, X. L. Zhu, et al., J. Mater Mech. Eng. **40**, 12-15 + 98 (2016).